

Impacts of Increased Atmospheric CO₂ on the Hydroclimate of the Western United States

JINWON KIM AND TAE-KOOK KIM*

Lawrence Berkeley National Laboratory, University of California, Berkeley, Berkeley, California

RAYMOND W. ARRITT

Department of Agronomy, Iowa State University, Ames, Iowa

NORMAN L. MILLER

Lawrence Berkeley National Laboratory, University of California, Berkeley, Berkeley, California

(Manuscript received 23 May 2001, in final form 20 November 2001)

ABSTRACT

Regional-scale projections of climate change signals due to increases in atmospheric CO₂ are generated for the western United States using a regional climate model (RCM) nested within two global scenarios from a GCM. The downscaled control climate improved the local accuracy of the GCM results substantially. The downscaled control climate is reasonably close to the results of an 8-yr regional climate hindcast using the same RCM nested within the NCEP–NCAR reanalysis, despite wet biases in high-elevation regions along the Pacific coast.

The downscaled near-surface temperature signal ranges from 3 to 5 K in the western United States. The projected warming signals generally increase with increasing elevation, consistent with earlier studies for the Swiss Alps and the northwestern United States. In addition to the snow–albedo feedback, seasonal variations of the low-level flow and soil moisture appear to play important roles in the spatial pattern of warming signals. Projected changes in precipitation characteristics are mainly associated with increased moisture fluxes from the Pacific Ocean and the increase in elevation of freezing levels during the cold season. Projected cold season precipitation increases substantially in mountainous areas along the Pacific Ocean. Most of the projected precipitation increase over the Sierra Nevada and the Cascades is in rainfall, while snowfall generally decreases except above 2500 m. Projected changes in summer rainfall are small. The snow budget signals are characterized by decreased (increased) cold season snowfall (snowmelt) and reduced snowmelt during spring and summer. The projected cold season runoff from high-elevation regions increases substantially in response to increased cold season rainfall and snowmelt, while the spring runoff decreases due to an earlier depletion of snow, except above 2500 m.

1. Introduction

The impacts of human-induced global climate change on regional hydrologic cycles are an important concern. Regional climate variations directly affect human society and the natural environment via water resources, frequency of natural disasters, energy consumption, and the health of ecosystems. Recently, a number of observational and global climate modeling studies show strong evidence that the observed tropospheric warming

trend is well correlated with the trend of increasing atmospheric CO₂, especially in the second half of the twentieth century (Santer et al. 1995). The Intergovernmental Panel on Climate Change (Houghton et al. 1995, hereafter IPCC 1995) provides a comprehensive summary of observational and modeling studies of the detection and attribution of global climate change associated with increased atmospheric CO₂ concentration.

Anthropogenic climate change has potentially important impacts on the western United States, which is among the most rapidly growing regions in the United States. The climate of the region is characterized by extreme seasonal contrasts in precipitation and strong orographic effects on the hydrologic cycle (Giorgi and Bates 1989; Kim 1997; Kim et al. 1998). Extreme seasonal contrasts in precipitation make it important to efficiently manage water storage facilities during the win-

* Current affiliation: Pukyung National University, Pusan, Korea.

Corresponding author address: Dr. Jinwon Kim, Department of Atmospheric Sciences, University of California, Los Angeles, Los Angeles, CA 90095-1565.
E-mail: jkim@atmos.ucla.edu.

ter to prevent flooding and to store water for the summer. Heavy precipitation and rapid streamflow response due to steep terrain often cause severe flood damage (Goodridge 1994; Soong and Kim 1996; Miller and Kim 1996; Kim et al. 1998; Groisman et al. 2001). The anticipated warming of the lower troposphere may affect the timing of snowmelt, which directly affects runoff and snowmelt-driven floods in mountainous areas in the spring (Cayan et al. 1993; Dettinger and Cayan 1995). This also has important implications for water resources, since snowpack accumulated during the cold season is an important source of water supply during the summer. Accurate projections of regional climate change signals associated with global climate change are crucial for long-term sustainable development via improved water resources management and better preparation for weather-related hazards.

Downscaling of climate change signals generated by general circulation models (GCMs) is an important step for assessing the impacts of climate change. Today's GCMs are typically run at spatial resolutions of a few hundred kilometers that are not sufficient to resolve local features that play important roles in shaping regional climate variability. For example, earlier studies by Giorgi et al. (1997) and Leung and Ghan (1999b, hereafter LG99) show that climate change signals depend strongly on elevation in mountainous regions. The Coastal Range, the Cascades, and the Sierra Nevada, which play a crucial role in precipitation and snow budget in the western United States, have spatial scales of 150 km or smaller, and cannot be resolved by GCMs. Dynamical downscaling based on nested modeling, in which a regional climate model (RCM) is nested within a GCM, has become an important tool to downscale global climate data for regional assessments. Recent RCM studies (Giorgi and Bates 1989; Giorgi et al. 1993, 1994, 1997; Giorgi and Shields 1999; Kim 1997; Kim et al. 1998, 2000; Kim 2001; Christensen et al. 1998; Leung and Ghan 1999a) show that RCMs can generate regional-scale features with reasonable accuracy from coarse-resolution global data. Dynamical downscaling can preserve physical and dynamical consistency among the downscaled variables better than statistical downscaling (e.g., Wilby et al. 1998; Kyriakidis et al. 2001). Hence, dynamical downscaling is especially useful for the western United States where complex terrain and physical processes determine important features of regional-scale climate variations.

Only a few regional-scale climate change projections have been made for the western United States using nested modeling so far. Giorgi et al. (1994, hereafter G94) investigated regional-scale climate change signals induced by increased CO₂ in two 3.5-yr simulations in which Pennsylvania State University–National Center for Atmospheric Research Mesoscale Model 4 (PSU–NCAR MM4) was nested within the NCAR Community Climate Model (CCM). G94 projects that cold season precipitation may increase by 20%–30% in the western

United States, while warm season rainfall may increase (decrease) in the northwestern (southwestern) region. They also project increases in the near-surface temperature of 3.7–4.7 K, with a larger increase during the cold season. In a recent study, in which a modified version of PSU–NCAR MM5 was nested within NCAR CCM, LG99 report climate change signals for the northwestern United States. LG99 projects smaller precipitation signals than G94, especially for most of the cold season (from October to February). A strong summer rainfall signal in LG99 may be an artifact of small summer rainfall in the control run. The temperature signal in LG99 is about 50% of G94. These and other early studies show that regional climate projections vary widely among the models, both GCMs and RCMs, employed for the projections. Hence, it is necessary to examine climate change signals from various global and regional models to obtain the range in which climate change signals are likely to reside.

Regional-scale climate change signals induced by increased atmospheric CO₂ are presented below using a nested modeling method. The main focus of the study is to quantify the effects of increased atmospheric CO₂ on the near-surface temperature, precipitation, snow budget, and runoff in the western United States. Below, we present the experimental design, which is followed by a brief description of the climate change signals from the driving GCM. Discussions of the projected regional-scale climate change signals follow.

2. Experimental design

For dynamical downscaling, an RCM is nested within global climate change scenarios from the second-generation coupled atmosphere–ocean model developed by the Hadley Centre for Climate Prediction and Research (HadCM2). HadCM2 is a finite-difference model on a grid of 2.5° lat × 3.75° lon with 19 atmospheric layers using a hybrid pressure– σ coordinate (Johns et al. 1997). The 20-layer ocean model uses the same horizontal grid as the atmospheric model. The HadCM2 fields used to drive the regional simulations are the horizontal winds, temperature, specific humidity, surface pressure, and sea surface temperature (SST) on the GCM's native grid so that its full resolution is preserved. The GCM fields used to drive our regional runs consist of 10-yr records from a control run with an effective greenhouse gas concentration similar to the late twentieth century, and a transient run in which greenhouse gas concentration increases approximately 1% yr⁻¹ from 1990. Aerosol effects are not included in the transient run. The 10-yr records for the control and transient runs nominally represent the years 2040–49, which is a few years before the time of CO₂ doubling of the 1990 level. As the control run shows little drift over multicentury timescales (Johns et al. 1997), the control climate for 2040–49 can also represent the GCM climatology for the late twentieth century. For details of HadCM2 and the two

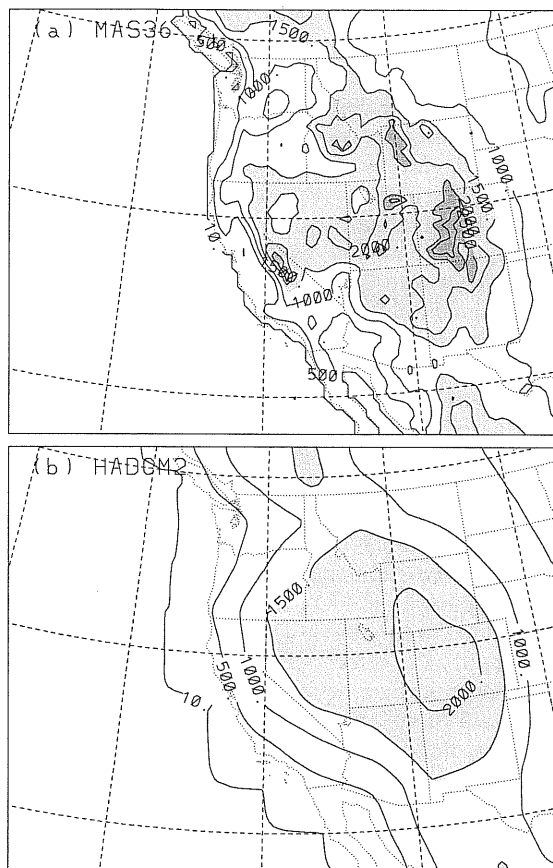


FIG. 1. Model terrain (m) of the western United States domain for the (a) regional (MAS-SPS) and (b) global (HadCM2) models. The GCM terrain was interpolated onto the MAS-SPS grid. Light (dark) shading indicates above 1500 m (2500 m).

global runs, see Mitchell et al. (1995) and Johns et al. (1997).

In the regional simulations, an RCM was driven by updating the lateral boundary conditions and SST at 12-h intervals using the GCM data interpolated onto the RCM grid. The Davis scheme (Davis 1976) is used to nudge the RCM field toward the GCM field along the lateral boundaries. The CO_2 concentration is fixed for the 10-yr period at the level of 340 and 540 ppmv for the control and transient runs, respectively. The RCM employed for this study is interactively coupled Mesoscale Atmospheric Simulation (MAS) and Soil-Plant-Snow (SPS) models. The RCM domain covers the western United States at a 36-km grid spacing on a Lambert-Conformal Conic projection (Fig. 1a), with 18 atmospheric layers between the surface and the 50-hPa level. For details of MAS and SPS, see Kim and Soong (1996), Soong and Kim (1996), Mahrt and Pan (1984), Pan and Mahrt (1987), and Kim and Ek (1995). Only a brief outline of the two models is presented below.

MAS is a primitive-equation, limited-area atmospheric model with a σ coordinate. The dependent variables of MAS are staggered on the Arakawa-C grid in the

horizontal, and on the Lorenz grid (Lorenz 1960) in the vertical. The advection equation is solved using the third-order accurate finite-difference scheme of Takacs (1985). Grid-scale condensation and precipitation are computed using a four-class version of the bulk microphysics scheme (Cho et al. 1989) after neglecting the graupel phase (Kim 1997). Atmospheric convection is calculated by the NCEP Simplified Arakawa-Schubert scheme (Pan and Wu 1995; Hong and Pan 1998). Solar and terrestrial radiative transfer is computed using the formulation of Harshvardhan et al. (1987), after the effects of ice- (Stephens 1978) and water-phase (Starr and Cox 1985) cloud particles are added. A two-layer version of SPS is coupled with MAS to compute the land surface processes. SPS predicts the volumetric soil moisture content (SMC), soil temperature, canopy water content, and water-equivalent snow depth (WESD). The temperature and specific humidity at the atmosphere-land interfaces are calculated diagnostically by iteratively solving a nonlinear form of the surface energy balance equation. The fraction of a grid box covered with green vegetation is prescribed for each month from fine-resolution satellite data (Gutman and Ignatov 1998). In this experiment, the thickness of the upper and lower soil layers are set to 5 and 195 cm, respectively.

3. The climate change signals in the GCM projection

The HadCM2 control run simulates seasonal and spatial variations of precipitation in the western United States reasonably well (Fig. 2). Compared to the European Centre for Medium-Range Weather Forecasts (ECMWF) reanalysis (Figs. 2e-f), the GCM control climate (Figs. 2a-d) is wetter for all seasons, especially in winter (January-March: JFM) and fall (OND). Even though the difference between the ECMWF and the GCM control run does not correspond to absolute GCM errors, it suggests that the GCM control run overestimates precipitation in the western United States. The GCM simulation also misses the characteristic precipitation distribution associated with mountain ranges along the Pacific coast. For a detailed evaluation of the HadCM2 control climate, readers are referred to Johns et al. (1997).

a. Atmospheric moisture content

The precipitable water (PW) signal in the HadCM2 projections suggests that the atmospheric moisture content increases in the western United States for all seasons (Fig. 3). The projected increase of the PW ranges from 2 to 6 mm within the RCM domain, with a larger increase in the southwestern region. Seasonally, the largest increase of the PW occurs during the summer (JAS), with the smallest increase in the spring (AMJ). The PW also increases by a large amount in the winter (JFM)

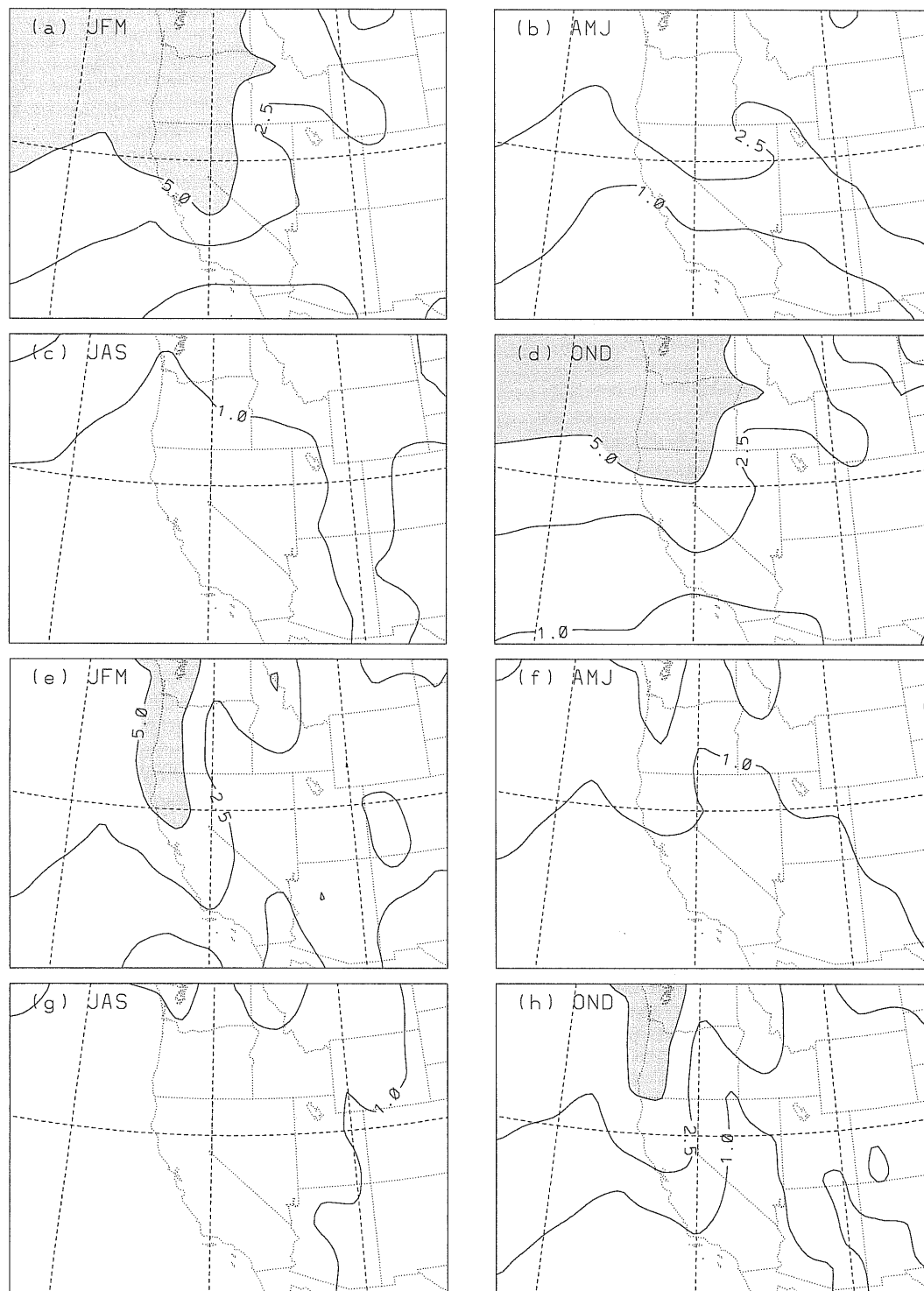


FIG. 2. Seasonal precipitation (mm day^{-1}) from (a)–(d) the GCM control run, and (e)–(h) the ECMWF reanalysis. Contours represent 1, 2.5, 5, and 10. The GCM climatology averages the control run precipitation for the 10-yr period 2040–2049. The ECMWF climatology is an average over the 14-yr period of 1979–92.

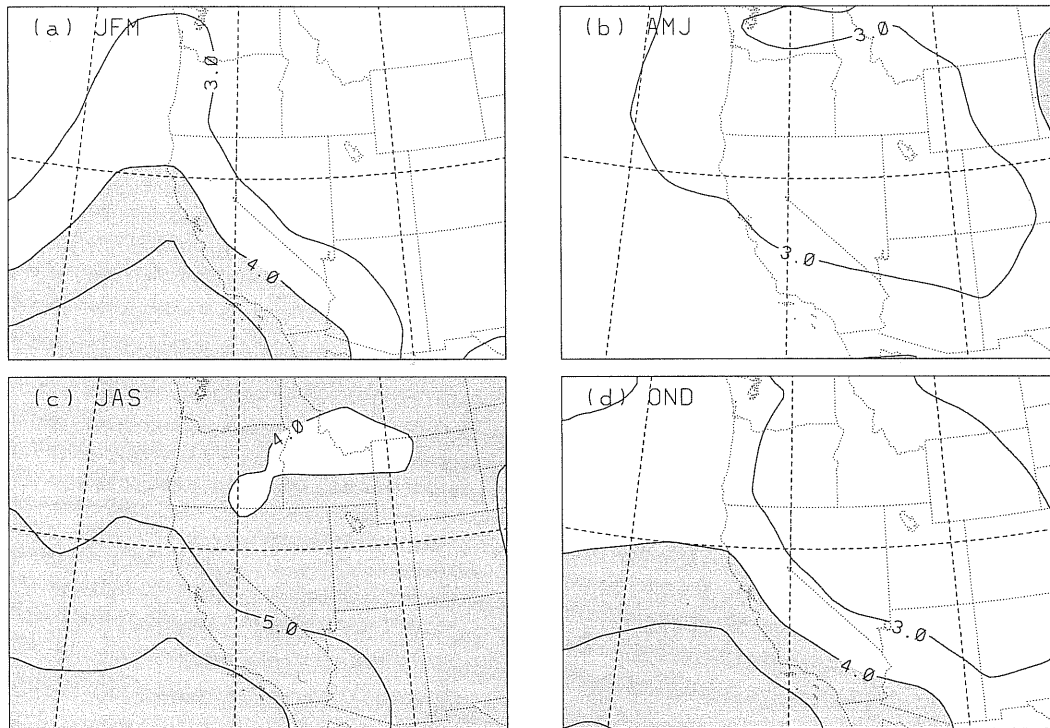


FIG. 3. The seasonal-mean precipitable water (PW) signal (mm) in the GCM results. Shading indicates the signal exceeds 4 mm.

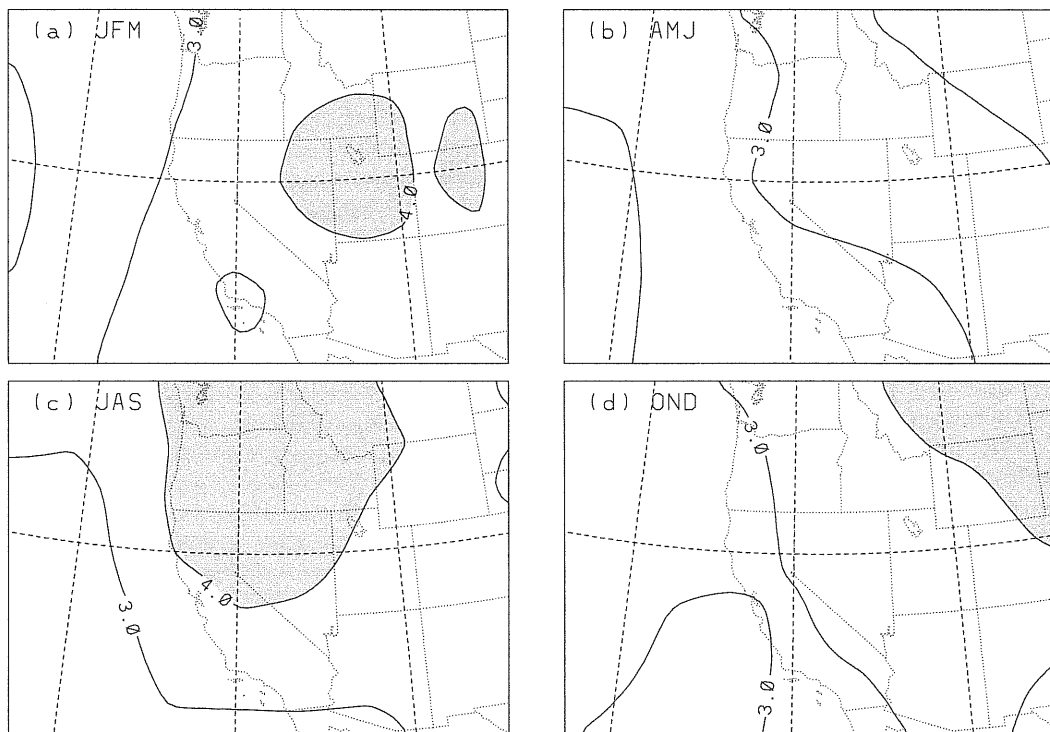


FIG. 4. Same as Fig. 3 but for the low-level air temperature (K). Shading indicates the signal exceeds 4 K.

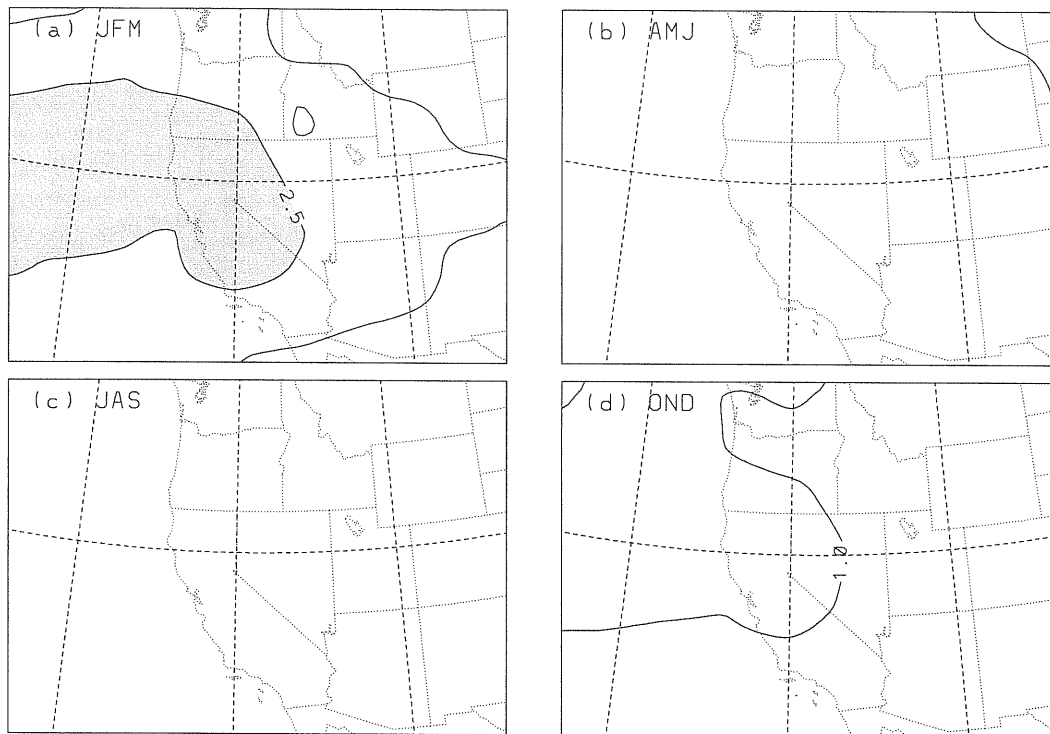


FIG. 5. Same as Fig. 3 but seasonal precipitation (mm day^{-1}). The shading indicates that the signal exceeds 2.5 mm day^{-1} .

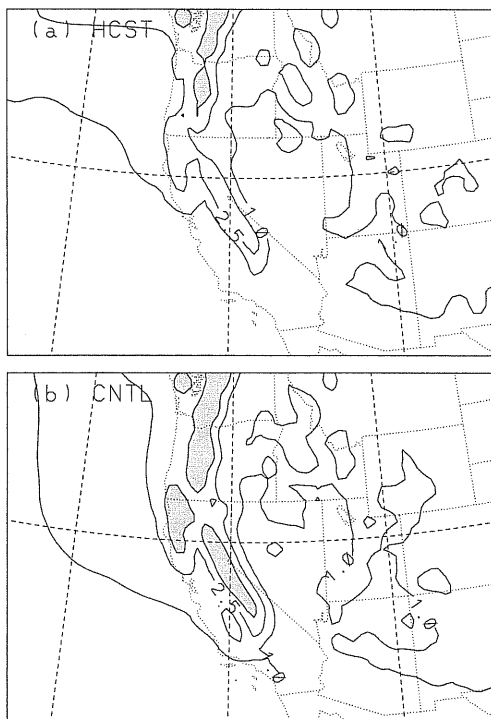


FIG. 6. The annual mean precipitation (mm day^{-1}) in (a) an 8-yr regional climate hindcast (1988–95) and (b) the 10-yr control run. The contour levels are 1, 2.5, 5, and 10. Shading indicates the annual mean precipitation exceeds 5 mm day^{-1} .

and fall (OND), especially along the Pacific coast. The HadCM2-projected PW signal is qualitatively consistent with an observed trend during the twentieth century, especially in the second half, which is suspected to be an effect of CO_2 -induced global warming trend (Elliott et al. 1995). Water vapor mixing ratio in the lowest HadCM2 layer shows a similar signal as the PW (not shown).

b. Near-surface air temperature

The GCM-projected near-surface temperature signal is in the range of 3–4 K in most of the western United States (Fig. 4), similar to the projections in G94 and LG99. The largest increase in the near-surface temperature occurs along the major mountain ranges and in the northwestern region. Note that the GCM terrain (Fig. 1b) resolves the Rocky Mountains, but does not resolve the Coastal Range, the Cascades, and the Sierra Nevada. The GCM-projected signals, therefore, do not capture the orographic effects of these mountain ranges along the Pacific Ocean, which play an important role in shaping the climate of the western United States (Kim 1997, 2001). The near-surface temperature increase is largest in winter and summer. In the winter, the strongest signals appear in high elevation areas, perhaps due to reduced snow cover. In the summer, the signal is strongest in the northwestern region (Washington, Oregon, northern California). Summertime low-level temperatures in this

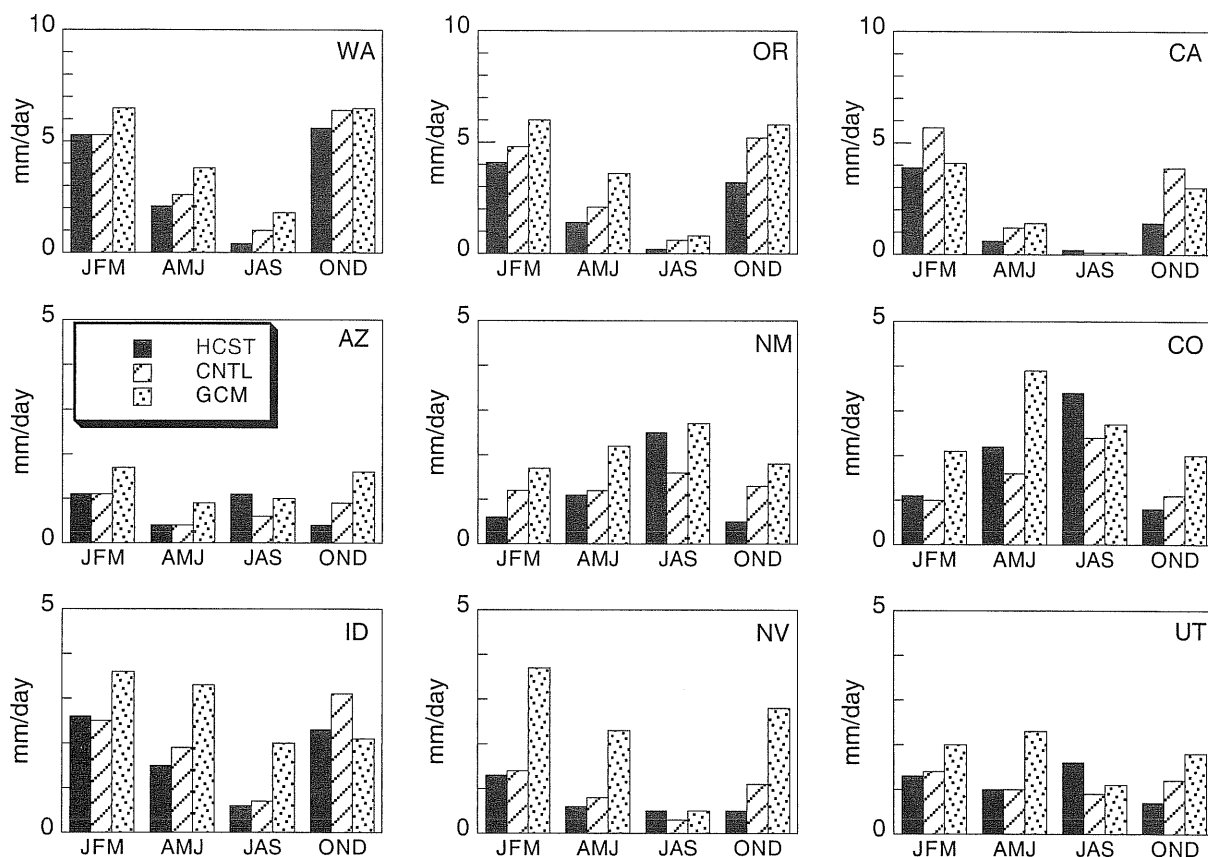


FIG. 7. Statewide seasonal-mean precipitation (mm day^{-1}) from the RCM hindcast (solid), the RCM control run (hatched), and the GCM control run (dotted). The months included in each season are winter (JFM), spring (AMJ), summer (JAS), and fall (OND).

region are sensitive to the snow budget and the occurrence of low-level northeasterly winds. In the spring and fall, the temperature signals are relatively weak, with the strongest ones appearing along the Rocky Mountains (highest GCM terrain) and in the northeastern part of the domain, respectively.

c. Precipitation

The GCM projection suggests a large increase of cold season precipitation in the western United States (Fig. 5). The most significant increase of precipitation occurs during the winter, when the signal exceeds 2.5 mm day^{-1} (over 50% of the control climate) in northern California (Fig. 5a). The fall precipitation signal shows a similar pattern as the winter. The largest precipitation signal during the winter and fall appears over the western slope of the GCM terrain. Despite increases in cold season precipitation, the projected snowfall decreases in most of the western United States due to higher freezing levels in warmer climate (not shown). The projected precipitation signals are smallest in the spring and summer. The summer rainfall suggests that increased CO_2 may have minimal effects on monsoon rainfall in Arizona and New Mexico where summer rainfall is unchanged

or decreases in the transient climate. Arritt et al. (2000) present the HadCM2-projected signals in the southwestern monsoon.

4. Downscaled control climate

We first compare precipitation and near-surface air temperature from the downscaled control run against a regional climate hindcast in which MAS-SPS was driven by NCEP reanalysis for the 8-yr period of 1988–95. Evaluations of the hindcast results show that MAS-SPS simulates regional climate features in the western United States with reasonable accuracy. Except for the large-scale forcing, the hindcast used the same RCM configuration, resolution, and domain as the regional climate projection. Hence, differences between the hindcast and the control run originate solely from the differences in the large-scale forcing between the reanalysis and the HadCM2 control climate. The differences, however, are not necessarily a measure of GCM errors. The regional climate hindcast and control run cover relatively short periods of 8 and 10 yr, respectively. Hence, the climatology from both the hindcast and the control runs does not account for interdecadal climate variability, which can strongly modulate

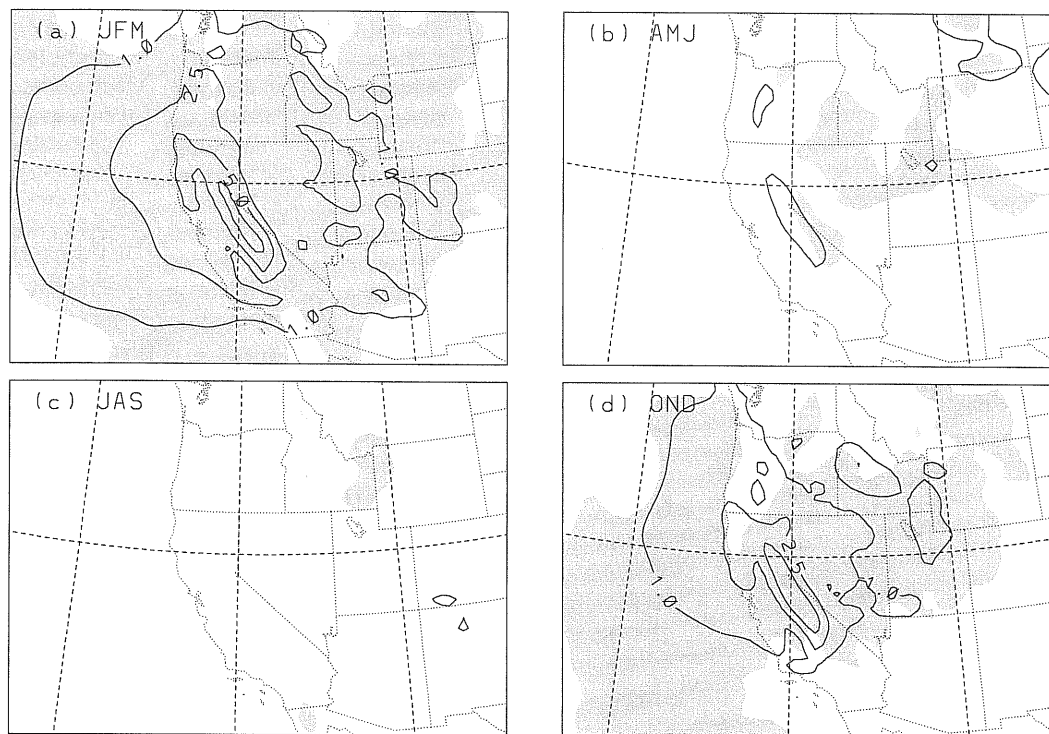


FIG. 8. The downscaled seasonal-mean precipitation signal (mm day^{-1}). The contours represent -1 , 1 , 2.5 , 5 , and 10 . Shading indicates the signal exceeds the 95% confidence level.

long-term regional climate variations (Chen et al. 1996; Akinremi and McGinn 1999).

The annual precipitation from the control run agrees well in pattern with the hindcast (Fig. 6). The control climate run overestimates precipitation in high elevation areas along the northern California Coastal Range, the Sierra Nevada, and the Cascades, that are the wettest regions in the western United States. Even though the control run overestimates both rainfall and snowfall in these regions, overestimation of rainfall is more pronounced (not shown). Statewide seasonal precipitation in the control run agrees reasonably with the hindcast (Fig. 7). The cold season (JFM, OND) precipitation in the control run generally exceeds that in the hindcast. During fall (OND), precipitation from the control run exceeds the hindcast in all states, especially in the southwest (California, Arizona, New Mexico, Nevada). Winter (JFM) precipitation in the control run is close to the hindcast, except in Oregon, California, and New Mexico. Summer rainfall in the control run is generally smaller than the hindcast, especially in the area affected by the North American summer monsoon (Colorado, Utah, Arizona, New Mexico). Even though summer rainfall in the control run is somewhat larger than the hindcast in the Pacific Northwest (Washington, Oregon), summer rainfall in this region is small in both simulations. The dynamically downscaled control climate agrees more closely with the hindcast than the GCM results (Fig. 7). Hence, dynamical downscaling can en-

hance applicability of the GCM-simulated climate data by improving their local accuracy.

The annual mean near-surface temperature (temperature at the 10-m level) in the downscaled control climate is also similar to the hindcast results (not shown). Differences between the hindcast and the control run are largest in high-elevation areas in eastern California, central Utah, and western Colorado. In these regions, the annual mean near-surface temperature in the control run is lower than the hindcast by 1–2 K, perhaps due to more snowfall in the control climate.

Despite differences between the downscaled control climate and the hindcast, available data are not sufficient to attempt to correct biases in the projected climate signals as the control run and the hindcast cover different and relatively short periods. Even though the GCM control run does not show noticeable drift over a few hundred years (Mitchell et al. 1995; Johns et al. 1997), it still contains interdecadal variability that cannot be represented adequately by 10-yr runs. As the downscaled control climate is reasonably close to the hindcast, the regional-scale climate change signals of increased CO_2 are estimated as differences between the values obtained from the control and transient runs in the discussions below.

5. Downscaled climate change signals

a. Precipitation

Figure 8 presents the downscaled seasonal precipitation signal. This signal is positive, that is, more precipitation

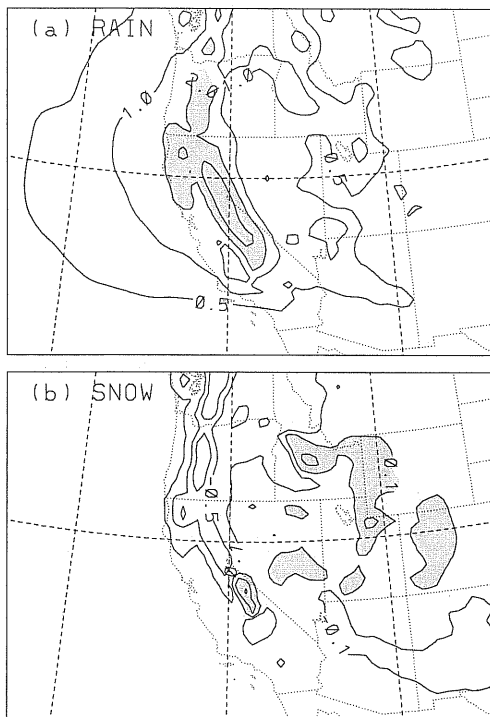


FIG. 9. The downscaled signals (mm day^{-1}) in the annual (a) rainfall and (b) snowfall. Shading indicates the annual mean rainfall (snowfall) exceeds 2 mm day^{-1} (0.1 mm day^{-1}).

in the transient run than in the control run, within the domain for all seasons. The strong precipitation signal along the Pacific Ocean is due to the fact that the high mountain ranges along the coast (the Coastal Range, the

Cascades, and the Sierra Nevada) are extremely efficient in extracting moisture from the atmosphere through orographic lifting (Chung et al. 1998). Much of the additional water vapor in the transient run precipitates out while passing over the mountain ranges. Due to the resulting rain shadow effects, the cold season precipitation signal decreases rapidly in the lee side of the mountain ranges. G94 also found similar orographic effects in the cold season precipitation signal in the western United States. The detailed spatial variation of the precipitation signal is crucial for assessing impacts of climate change on the surface hydrologic cycle, but is not available in the GCM data (Fig. 5) due to a coarse spatial resolution. Precipitation increases are also clear in the northern part of the domain (Idaho, Montana, Wyoming), as well as in western Nevada and central parts of Utah and Arizona. Precipitation may decrease slightly in New Mexico in the altered climate; however, statistical confidence of the precipitation signal is well below the 95% level in this region. Increased precipitation in the transient run is mainly due to increased rainfall (Fig. 9). Rainfall increases substantially in the regions where the precipitation signal is largest (Fig. 9a). Snowfall generally decreases except in a few areas where the model terrain exceeds 2500 m (Fig. 9b). The decrease in snowfall is associated with elevated freezing levels due to a warmer lower troposphere in the transient run (Kim 2001). A regional climate model study by LG99 suggests similar snowfall changes across 2000–2500 m in the northwestern United States due to increased atmospheric CO_2 .

Figure 10 compares the seasonal mean statewide precipitation in the control and transient runs. The winter precipitation increases in all states, most notably in California, Nevada, and Arizona, where the GCM projected

TABLE 1. Standard deviation of seasonal precipitation (mm day^{-1}) in the control (CNTL) and the transient (TRAN) runs. The numbers in parenthesis are the coefficient of variation (dimensionless: std dev mean^{-1}).

| | Winter (JFM) | | Spring (AMJ) | | Summer (JAS) | | Fall (OND) | |
|-----------------|----------------|----------------|----------------|----------------|----------------|----------------|----------------|----------------|
| | CNTL | TRAN | CNTL | TRAN | CNTL | TRAN | CNTL | TRAN |
| Arizona (AZ) | 0.97 (0.85) | 1.42 (0.65) | 0.21 (0.57) | 0.35 (0.68) | 0.41 (0.73) | 0.34 (0.60) | 0.71 (0.80) | 0.57 (0.54) |
| California (CA) | 2.48 (0.44) | 3.03 (0.31) | 0.51 (0.43) | 0.64 (0.39) | 0.13 (1.17) | 0.70 (1.72) | 1.43 (0.36) | 2.91 (0.46) |
| Colorado (CO) | 0.46 (0.47) | 0.55 (0.33) | 0.42 (0.26) | 0.58 (0.27) | 0.61 (0.25) | 0.57 (0.27) | 0.31 (0.30) | 0.43 (0.32) |
| Idaho (ID) | 0.69 (0.27) | 1.16 (0.30) | 0.42 (0.22) | 0.62 (0.26) | 0.21 (0.32) | 0.49 (0.52) | 0.88 (0.28) | 0.94 (0.23) |
| Montana (MT) | 0.38 (0.48) | 0.24 (0.21) | 0.59 (0.24) | 1.14 (0.37) | 0.49 (0.33) | 0.51 (0.34) | 0.23 (0.23) | 0.31 (0.23) |
| New Mexico (NM) | 0.60 (0.48) | 0.76 (0.57) | 0.52 (0.42) | 0.56 (0.49) | 0.63 (0.40) | 0.62 (0.44) | 0.43 (0.33) | 0.56 (0.45) |
| Nevada (NV) | 0.67 (0.46) | 0.97 (0.31) | 0.16 (0.21) | 0.43 (0.38) | 0.20 (0.71) | 0.33 (0.93) | 0.45 (0.39) | 1.11 (0.48) |
| Oregon (OR) | 0.93 (0.19) | 1.96 (0.29) | 0.58 (0.28) | 0.91 (0.34) | 0.19 (0.33) | 0.48 (0.64) | 1.69 (0.33) | 1.41 (0.22) |
| Utah (UT) | 0.62 (0.45) | 0.83 (0.31) | 0.17 (0.17) | 0.46 (0.35) | 0.63 (0.68) | 0.48 (0.51) | 0.38 (0.31) | 0.90 (0.45) |
| Washington (WA) | 1.79 (0.34) | 2.24 (0.34) | 0.87 (0.33) | 0.72 (0.27) | 0.29 (0.28) | 0.57 (0.50) | 1.67 (0.26) | 1.55 (0.25) |
| Wyoming (WY) | 0.19 (0.24) | 0.26 (0.20) | 0.38 (0.17) | 0.69 (0.24) | 0.54 (0.35) | 0.62 (0.38) | 0.17 (0.18) | 0.36 (0.25) |

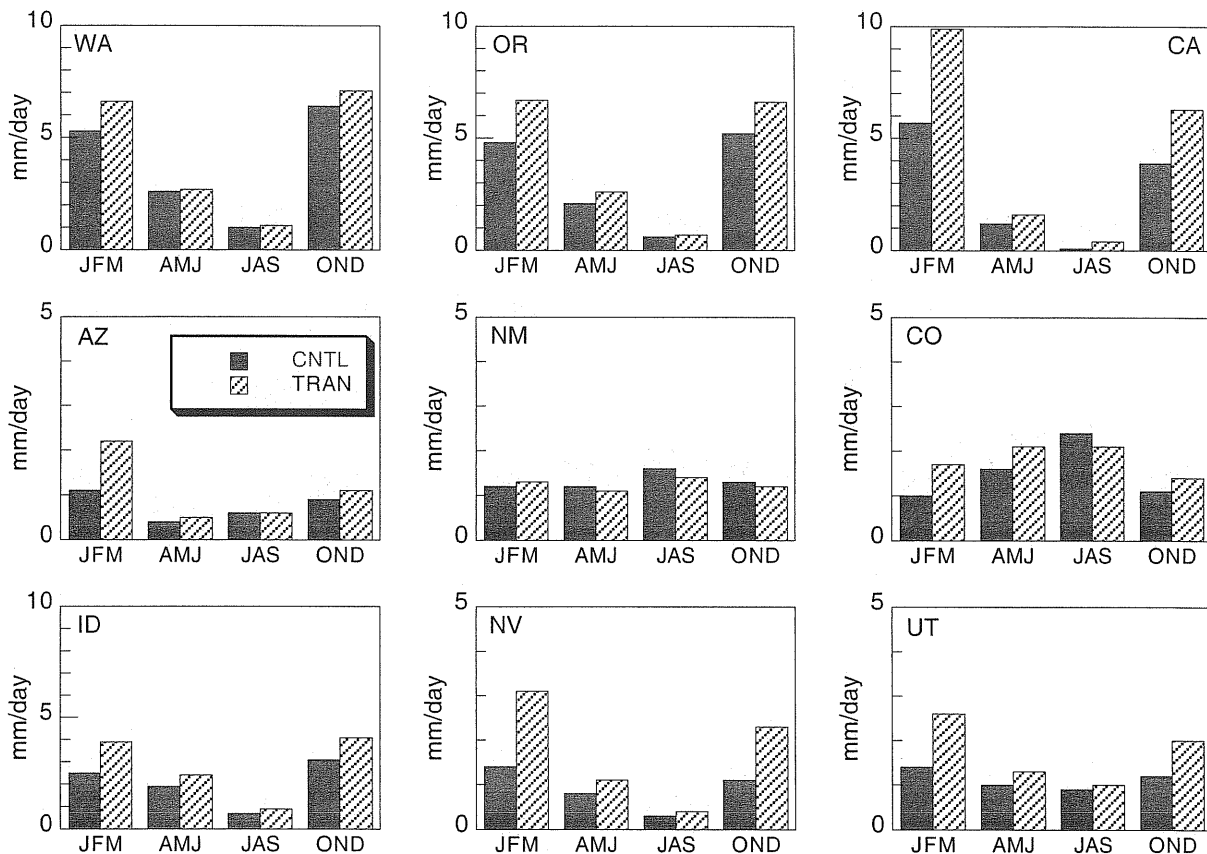


FIG. 10. The downscaled statewide seasonal precipitation (mm day^{-1}) in the control (solid) and the transient (hatched) runs.

the largest increases in the PW (Fig. 3), low-level mixing ratio, and precipitation (Fig. 5). The fall precipitation signal is also positive in most states, but it is smaller than the winter signal. The warm season (AMJ, JAS) signal is also generally positive, but it is weaker than the cold season (JFM, OND) and its statistical significance is low (Figs. 8b,c). The summer rainfall signals in the region affected by the North American summer monsoon circulation are either very small (Arizona) or negative (New Mexico, Colorado).

Projected changes in precipitation characteristics are closely related to low-level temperature, through the altitudes of freezing levels and seasonal variation of the low-level temperature, in addition to increased atmospheric moisture content in the transient run (Kim 2001). Increases in the cold season precipitation are mainly due to increased rainfall. Cold season rainfall increases in all states (Fig. 11a) in response to increased large-scale moisture flux and higher freezing levels in the transient run. Snowfall decreases throughout the cold season along the Pacific Ocean (Washington, Oregon, California) and in the southwestern United States (Arizona, New Mexico), which stays warm during the winter (Fig. 9b). In this region, snowfall increases only above the 2500-m level. In the interior (Colorado, Idaho, Nevada, Utah), snowfall increases in the winter, as the wintertime low-level temperature remains

largely below freezing despite the projected warming in the transient run. Fall snowfall, however, decreases or is unchanged in the interior region as the low-level temperature is warmer than in winter.

The interannual variability of seasonal precipitation, measured by the standard deviation of seasonal values (σ_{PR}) over the 10-yr period (Table 1), generally coincides with the seasonal precipitation signal. In each state, σ_{PR} increases for the seasons in which seasonal precipitation also increases, implying that precipitation differences between dry and wet years increase in an increased CO_2 climate. Also shown in Table 1, in the parenthesis, is the corresponding coefficient of variation (CVR) defined as the ratio between σ_{PR} and the climatological mean. Unlike σ_{PR} that is generally larger in the transient run, the CVR in the transient run is often smaller than in the control climate. Annual precipitation in the transient run does not show a discernable temporal trend over the 10-yr period, either in individual states or over the entire land surface within the domain.

b. Near-surface temperature

The seasonal mean temperature signal ranges from 3 to 5 K (Fig. 12) and exceeds the 95% confidence level almost everywhere within the domain. In the summer,

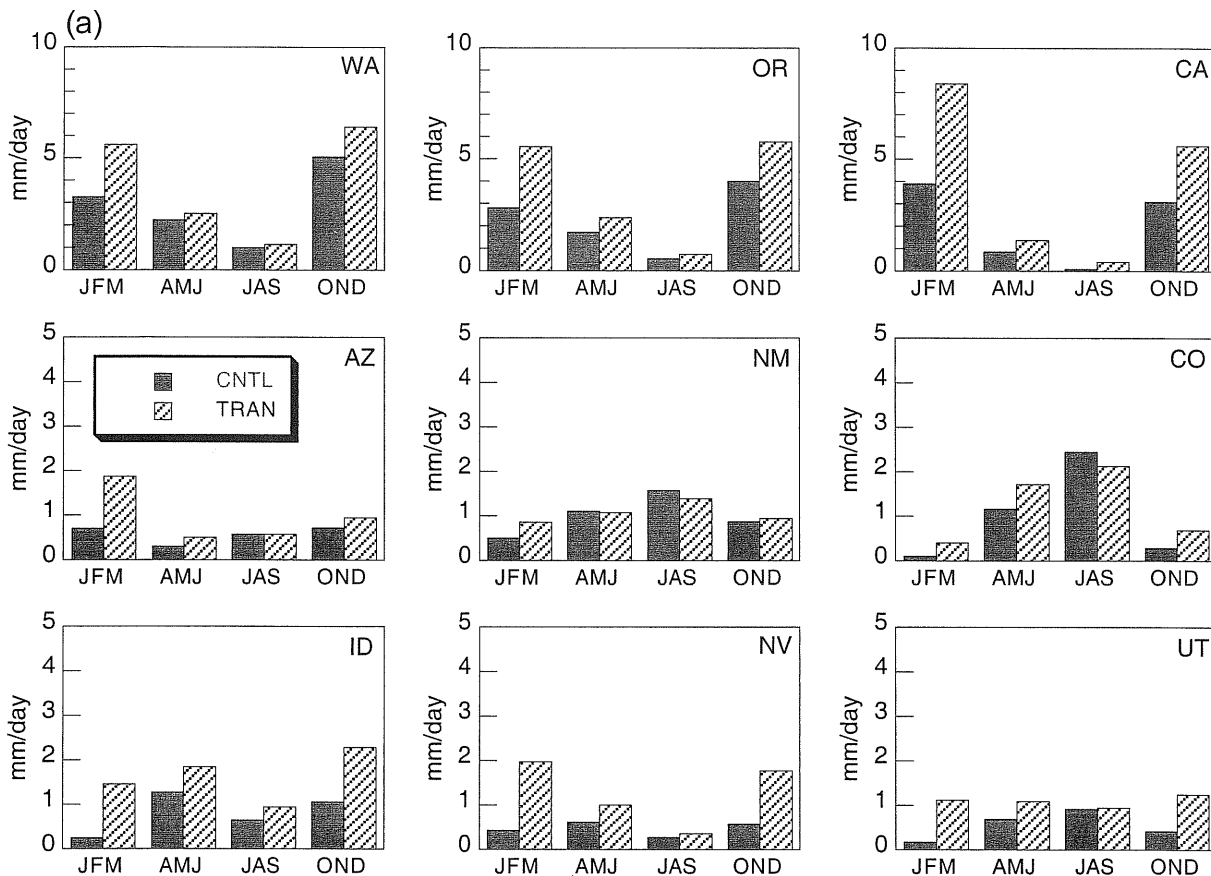


FIG. 11. The downscaled statewide seasonal (a) rainfall and (b) snowfall (mm day^{-1}) in the control (solid) and transient (hatched) runs.

the largest warming signal appears in the northwestern region (Washington, Oregon, Idaho, Nevada, northern California), where the surface temperature increases by over 4 K. A similar temperature increase also appears in western Colorado. Smaller increases of 2–3 K appear in the Pacific coast region, west of the Cascades and the Sierra Nevada, in winter, spring, and fall. This suggests that the projected warming signal is also affected by the seasonal variations of the low-level wind field. During the latter three seasons, low-level winds are generally from the west, and bring cooler marine air into the coastal regions west of the Cascades and the Sierra Nevada. During the summer, frequent low-level northeasterly winds, that bring warm air from the interior into the coastal areas, are suspected to cause the strong warming signal in the northwestern region. Similar seasonal variations of the warming pattern also appear in LG99.

As in the GCM results, the downscaled warming signals depend strongly on terrain elevation. Figure 13 shows the signals in the daily mean (TBAR: solid), minimum (TMIN: dashed line/open circles), and maximum (TMAX: dashed line/solid square) near-surface temperature in three terrain elevation ranges (Table 2). The annual and seasonal mean warming signals in all three

daily temperature fields increase with height except in California, where the warming signal above the 2000-m level is smaller than in regions between 1000 and 2000 m, except in summer (Fig. 13). The elevation-dependent temperature signal is mainly related to reduced winter snowfall and spring–summer snow cover in high altitudes in the altered climate. The snow–albedo feedback plays an important role in determining low-level temperature in high-elevation regions. As snow cover at the end of the winter is smaller in the transient run, albedo is reduced in spring and early summer in high elevations. The effects of snow cover on high-elevation temperature signals are well summarized by IPCC 1995 and Giorgi et al. (1997). For a given elevation range, the TMIN signals are larger than both the TBAR and TMAX signals, in general. Differences between the TMIN and TBAR signals are smaller in the summer than in the winter (Fig. 13). Note that the summertime signals show additional complexity in dry regions. In the interior region (Arizona, Colorado), TMAX increases more than TMIN during the summer. This may be related to the changes in winter rainfall. As summer rainfall decreases, evapotranspiration (or latent heat flux) decreases. Increased daytime sensible

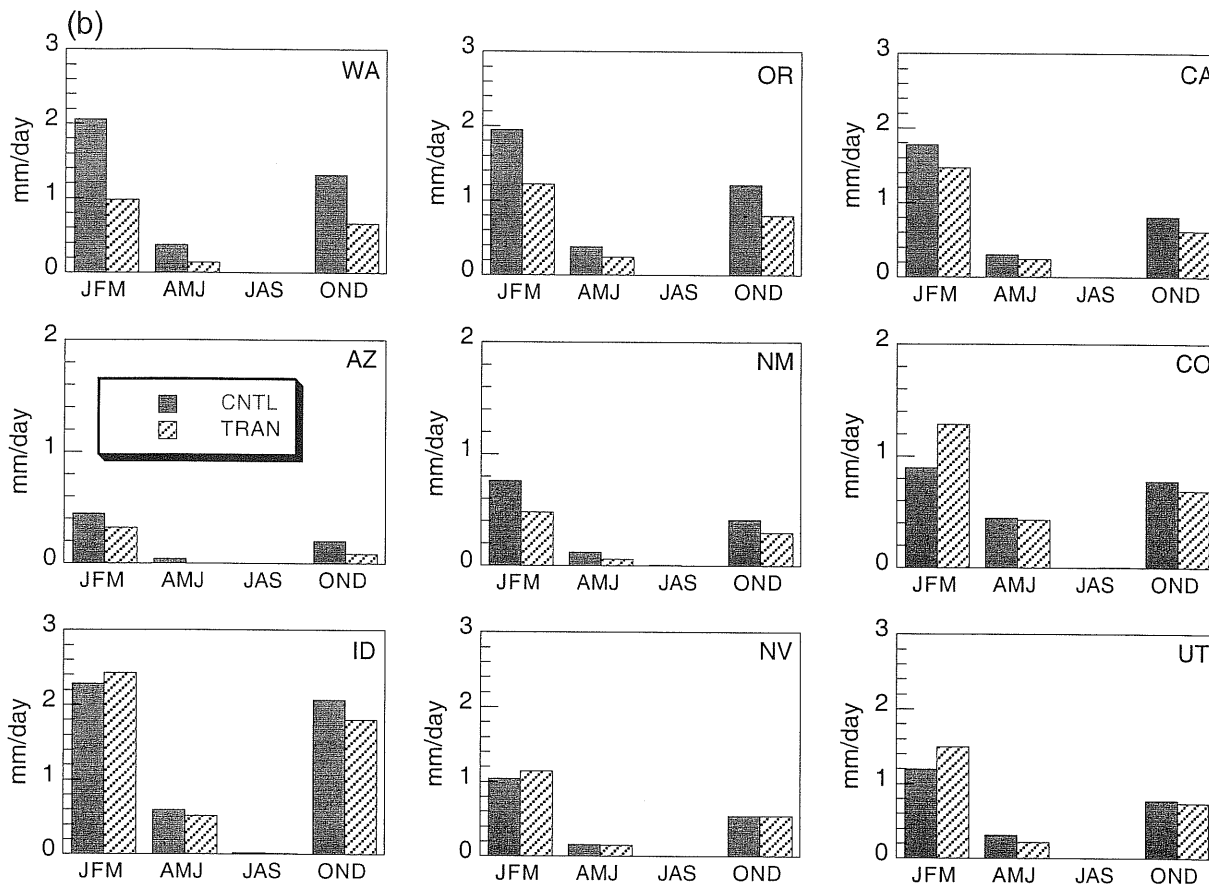


FIG. 11. (Continued)

heat flux tends to increase the daily maximum temperature.

Unlike the precipitation signal, interannual variability in the near-surface temperature signal, averaged over the land surface, in the transient run shows a discernable temporal trend over the 10-yr period (not shown). The annual mean low-level temperature increases at a rate of 0.033 K yr^{-1} , although interannual variation is large (standard deviation of 0.67 K). The TMIN trend (0.036 K yr^{-1}) is larger than the TMAX trend (0.020 K yr^{-1}).

c. Effects on snow

Increases in the lower-tropospheric temperature have significant impacts on the snow budget in the western United States as the freezing level migrates to higher altitudes and snowmelt is accelerated, especially during the winter. The effects of the warming on snowfall are

largest in the elevation range between the 1000- and 2000-m levels, especially in the Pacific coast region. In this region, this elevation range includes the Cascades, northern California, and the Sierra Nevada (Fig. 9b), which are important for the water supply in spring and summer.

Figures 14a,b presents the seasonal mean snowmelt signal for winter and spring, respectively. The shading indicates that snowmelt increases by 0.2 mm day^{-1} or more in the altered climate. The projected snowmelt signal appears to exceed the 95% confidence level in high-elevation areas in the Sierra Nevada and the Rocky Mountains where the projected signals are large. During the winter, snowmelt increases in most high-elevation areas in the Sierra Nevada, Cascades, and the Rocky Mountains due to warmer near-surface temperatures (Fig. 14a). The enhanced winter snowmelt depletes most of snow cover by the end of the winter. As a result,

TABLE 2. Number of grid points in each model terrain elevation range.

| Elevation ranges | Arizona | California | Colorado | Oregon |
|-----------------------------------|---------|------------|----------|--------|
| Low: Below 1 km | 64 | 179 | 0 | 54 |
| Middle: Above 1 km and below 2 km | 126 | 95 | 86 | 30 |
| High: Above 2 km | 18 | 16 | 99 | 0 |

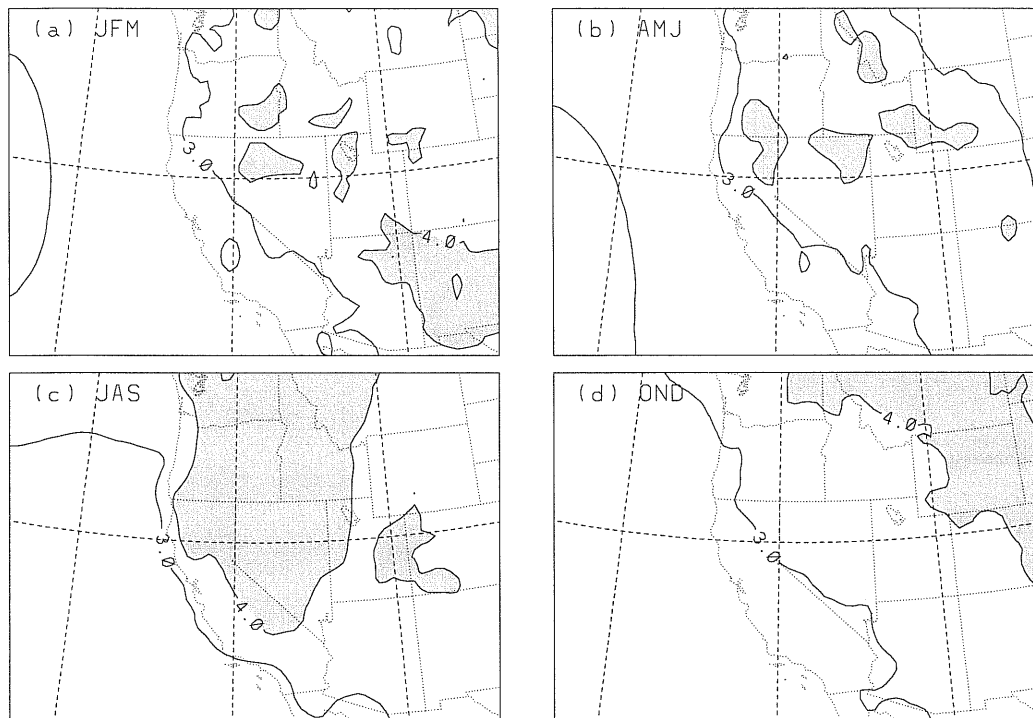
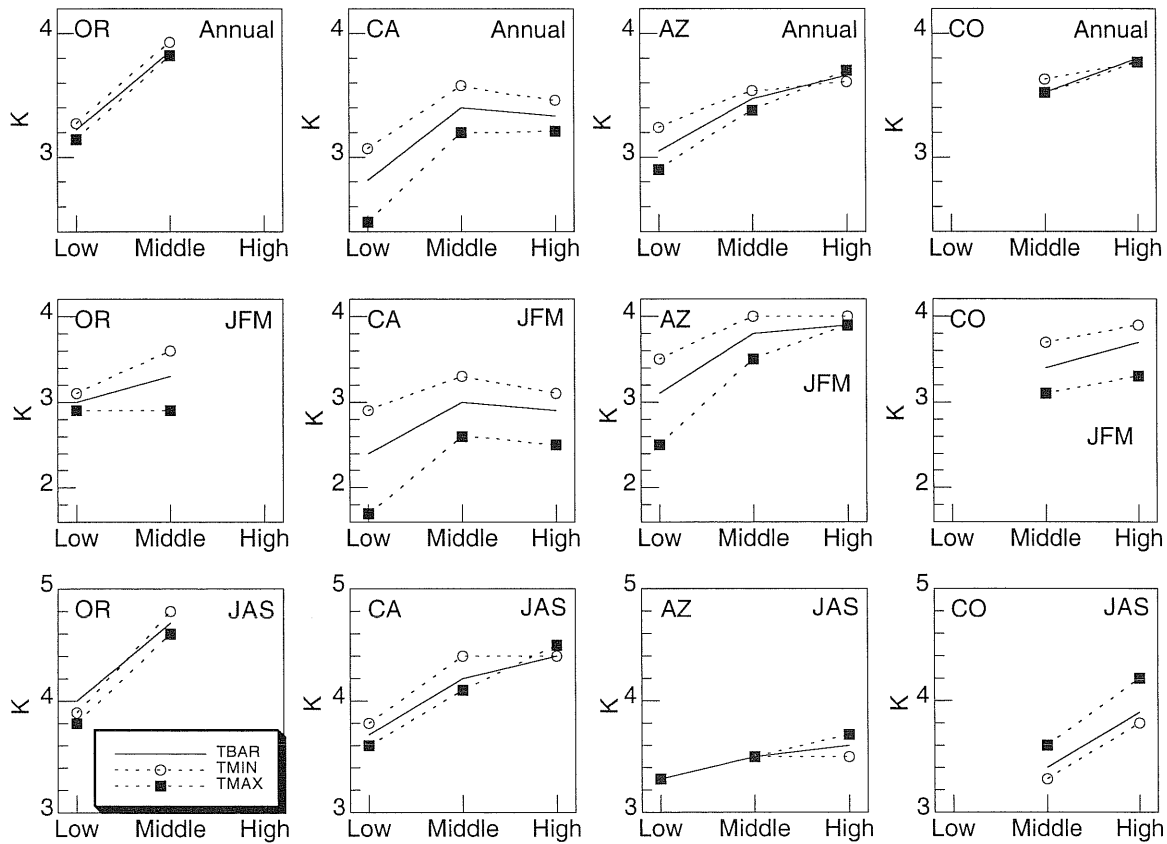


FIG. 12. The downscaled seasonal mean near-surface air temperature signal (K). Shading indicates the signal exceeds 4 K.



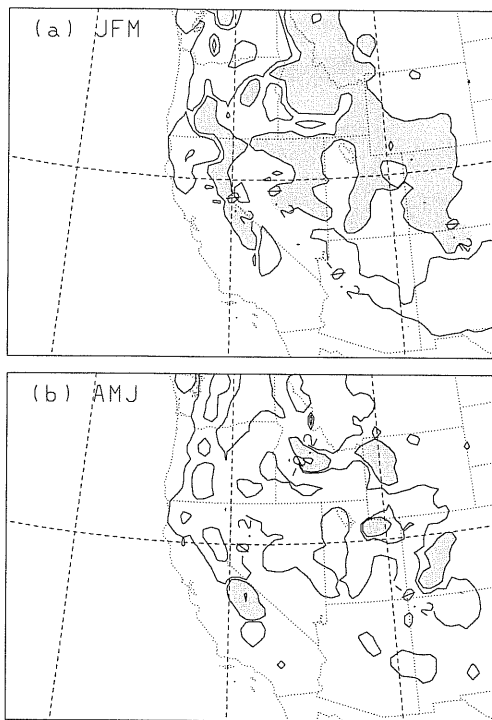


FIG. 14. The downscaled snowmelt signal (mm day^{-1}) for (a) winter (JFM) and (b) spring (AMJ). The contour levels are -2 , -0.2 , 0.2 , and 2 . Shading indicates the signal exceeds 0.2 mm day^{-1} .

spring snowmelt is reduced substantially in most high elevation regions except in very high elevations above 2500 m. In the very high elevation areas, near-surface temperatures remain largely below freezing during the winter despite the warming. As a result, snowmelt in the transient run is close to the control run. The cold surface temperature in very high elevations also reduces the tendency for precipitation to fall as rain instead of snow. Small changes in snowmelt and increased snowfall result in increased snow cover during the winter in the very high elevation regions. Hence, spring–summer snowmelt signal is positive above 2500 m.

Decreased snowfall and enhanced cold season snowmelt substantially reduce the number of days with snow cover. This tendency is most pronounced in the Pacific Northwest and New Mexico, in the elevation range between 1000 and 2500 m, where the annual mean snow cover days are reduced by more than 30 days in the transient run (Fig. 15). The projected changes in the snow cover days are small in the areas where the model terrain is below 1000 m (small number of snow cover days in the control run) or above 2500 m (temperature

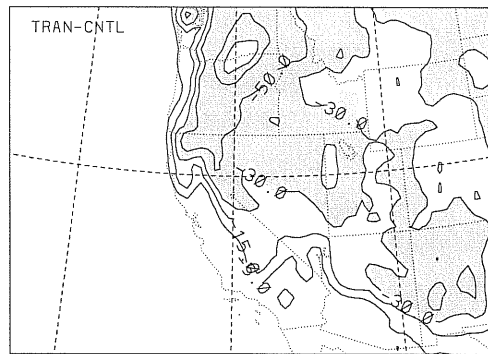


FIG. 15. Difference in the annual mean snowcover days between the transient and control runs. The contour levels represent -5 , -15 , -30 , and -50 days. Shading indicates the annual mean snow cover days are reduced by more than 30 days in the transient run.

is cold enough to sustain cold season snow cover in the transient run).

d. Runoff signals

The runoff signal (Fig. 16) reflects the changes in precipitation characteristics and snowmelt. Note that runoff in this study is a sum of surface runoff and drainage into deep soil through the bottom of the model soil layer, and does not correspond exactly to streamflow. Cold season (JFM, OND) runoff increases in most of the western United States, especially in high-elevation regions along the Pacific Ocean, in response to increased rainfall and snowmelt. In this region, the runoff signal also exceeds the 95% confidence level during the cold season. Spring runoff from the Cascades and the northern Sierra Nevada decreases by more than 0.5 mm day^{-1} due to reduced spring snowmelt. Increased spring runoff occurs in the northern California Coastal Range and in very high elevations in the southern Sierra Nevada and the Rocky Mountains due to increased spring rainfall (over the northern California Coastal Range) and increased snowmelt (in very high-elevation regions), as discussed above. A positive summertime runoff signal occurs only in the southern Sierra Nevada above the 2500-m level, where snowfall increases. Analogous to the seasonal precipitation signal (Fig. 8), statistical confidence of warm season runoff signals is much smaller than the cold season.

6. Conclusions and discussion

Regional-scale climate change signals in the western United States induced by increased atmospheric CO_2

←

FIG. 13. The downscaled signals (K) in TBAR (solid lines), TMIN (dashed lines with open circles), and TMAX (dashed lines with solid squares) in three elevation ranges for all seasons (annual), winter (JFM), and summer (JAS). See Table 2 to for the elevation ranges and the number of grid points in each elevation range.

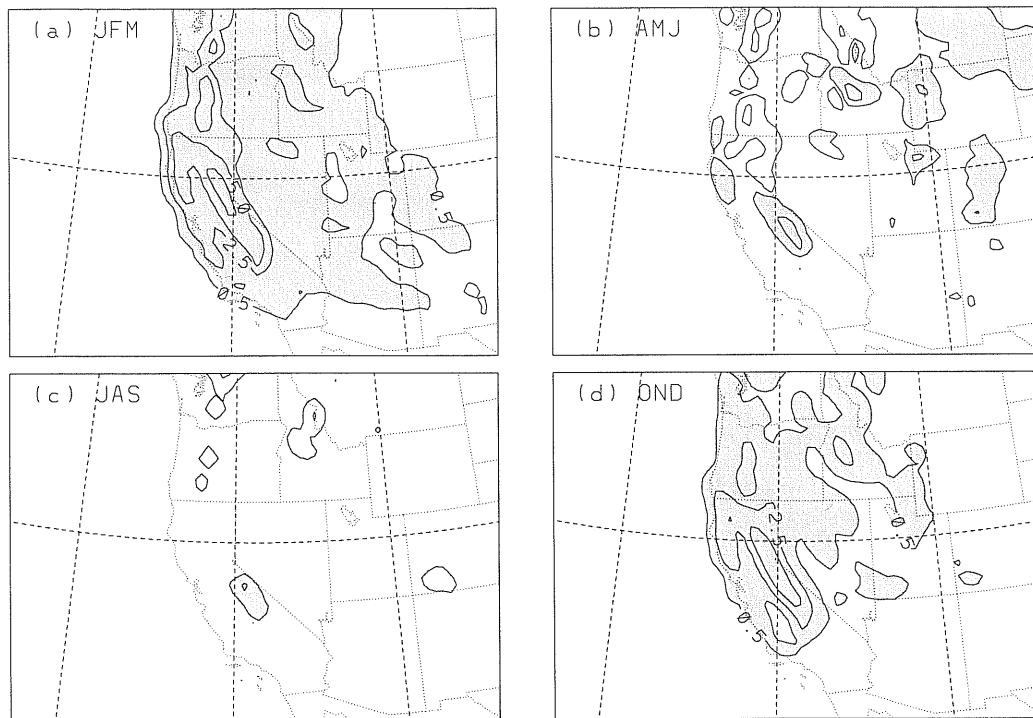


FIG. 16. The downscaled seasonal mean runoff signal (mm day^{-1}). The contour levels are -2.5 , -0.5 , 0.5 , 2.5 , 5 , and 10 . Shading indicates the signal exceeds 0.5 mm day^{-1} .

are investigated using an RCM nested within global climate change scenarios generated by HadCM2. The GCM simulations project a warming of 3–5 K, and large increases in the precipitable water and low-level water vapor under elevated CO_2 concentrations. The effects of increased atmospheric water vapor on precipitation are most pronounced along the Pacific coast during the winter. The GCM-generated signals, however, possess limited applicability for climate change and impact assessment studies due to their coarse spatial resolutions.

The dynamically downscaled climate change signals from MAS–SPS nested within the global climate change scenarios reproduce the general features of the GCM-generated signals, both in spatial patterns and magnitudes. The RCM produces richer spatial details of the signals associated with the region's complex terrain. The RCM projections show clearly the precipitation maxima over the Coastal range and the Sierra Nevada with a rainshadow region between them. Such details are not available in the GCM results. Improved spatial details generated by the RCM enhance applicability of the projected climate change signals for climate impact assessments substantially.

The downscaled near-surface temperature signal ranges from 3 to 5 K in the western United States, similar to the values projected in G94 and LG99. The projected temperature signals are affected by regional elements including seasonal variations of the low-level winds, snow budget, and summer rainfall changes through temperature advection, albedo, and surface en-

ergy budget, respectively, in addition to the large-scale climate changes. The low-level warming signal tends to increase with terrain elevation, as decreased high-elevation snowcover reduces albedo, especially during the winter and spring. Diurnal temperature variations in the interior region are also affected by reduced summer monsoon rainfall. As summer rainfall decreases, surface latent heat fluxes (sensible heat fluxes) decrease (increase). Increased sensible heat fluxes are favorable for higher daily maximum temperatures for a given amount of insolation. Hence, the daily maximum temperature increase is larger than the daily minimum temperature increase, resulting in increased diurnal cycles in the interior part of the western United States during the summer.

The downscaled climate change signals suggest a large increase in cold season precipitation, especially in the mountainous regions along the Pacific coast, in response to increased cold season moisture flux from the Pacific Ocean. In the Sierra Nevada and the northern California Coastal Range, the cold season precipitation increase is about 100% of the control climate. An important signal is that much of the projected precipitation increase in the Sierra Nevada and the Cascades is in rainfall due to elevated freezing levels that turns snowfall into rainfall. As a result, snowfall decreases in most of the mountainous regions, despite increased moisture flux into the region, except above 2500 m. In the interior region, increased snowfall is projected for high-elevation regions along the Rocky Mountains. The summer

rainfall signal is generally small and positive within the domain, except in the region affected by the North American summer monsoon (Arizona, New Mexico, Colorado), where summer rainfall decreases.

The projected surface snow budget signal is characterized by decreased snowfall, increased cold season snowmelt, and decreases in spring snowmelt in most mountainous regions below 2000 m, most significantly along the Pacific coast. Due to reduced snowfall and increased cold season snowmelt, the projected snow cover decreases in most mountainous areas at the beginning of the spring, except above 2500 m. Spring snowmelt increases only in very high elevation areas in the southern Sierra Nevada and the Rocky Mountains. Cold season runoff in high-elevation regions increases due to increases in cold season rainfall and snowmelt. In response to reduced snowfall and early snowmelt, spring runoff from mountainous regions decreases, except in very high-elevation regions. Runoff increases in the northern California Coastal Range mainly due to increased spring rainfall.

Downscaled climate change signals obtained in this study suggest that global climate change induced by increased CO₂ may substantially alter the hydrologic cycle in the western United States. Increases in cold season rainfall and snowmelt imply higher flood frequency during the cold season. Reduced spring snowmelt reduces water resources and hydropower generation during the dry season from late spring to early fall. The climate change signal obtained in this study qualitatively agrees with earlier studies (e.g., IPCC 1995; Giorgi et al. 1994, 1997; LG99), but the magnitudes of the projected signals often show large differences, especially in precipitation. Existing studies, including this one, cannot conclusively quantify the climate change signals due to increased CO₂, since climate change signals vary widely among the GCMs and RCMs employed to project climate change signals. An ensemble projection employing multiple RCMs and GCMs may help to obtain the range in which climate change signals are likely to reside.

Acknowledgments. We thank David Hassell and Richard Jones at the Hadley Centre, United Kingdom, for the global data from the HadCM2 climate runs, and John D. Farrara, Sungjoon Koo, and Susan Kembell-Cook for careful reviews and comments. This work was supported by the LBNL-DOE (LDRD-366139), NASA-EOS/IDS (NAG5-11363), NASA-RESAC (NS7291), the Electric Power Research Institute and by NSF (ATM-9909650). Work for the U.S. Dept. of Energy was done under Contract DE-AC03-76SF00098.

REFERENCES

- Akinremi, O. O., and S. M. McGinn, 1999: Precipitation trends on the Canadian prairies. *J. Climate*, **12**, 2996–3003.
- Arritt, R. W., D. C. Goering, and C. J. Anderson, 2000: The North American monsoon system in the Hadley Centre coupled ocean-atmosphere GCM. *Geophys. Res. Lett.*, **27**, 565–568.
- Cayan, D. R., L. G. Riddle, and E. Aguado, 1993: The influence of precipitation and temperature on seasonal streamflow in California. *Water Resour. Res.*, **29**, 1127–1140.
- Chen, T., J. Chen, and C. Winkle, 1996: Interdecadal variation in U.S. Pacific coast precipitation over the past four decades. *Bull. Amer. Meteor. Soc.*, **77**, 1197–1205.
- Cho, H.-R., M. Niewiadomski, and J. Iribarne, 1989: A model of the effect of cumulus clouds on the redistribution and transformation of pollutants. *J. Geophys. Res.*, **94** (D10), 12 895–12 910.
- Christensen, O. B., J. H. Christensen, B. Machenhauer, and M. Botzet, 1998: Very high-resolution regional climate simulations over Scandinavia—Present climate. *J. Climate*, **11**, 3204–3229.
- Chung, J.-S., J. Kim, J.-H. Oh, and W.-T. Kwon, 1998: Effects of ice-phase physics in simulating grid-scale precipitation. *Korean J. Atmos. Sci.*, **1**, 94–103.
- Davis, H., 1976: A lateral boundary formulation for multi-level prediction models. *Quart. J. Roy. Meteor. Soc.*, **102**, 404–418.
- Dettinger, M. D., and D. R. Cayan, 1995: Large-scale atmospheric forcing of recent trends toward early snowmelt runoff in California. *J. Climate*, **8**, 606–623.
- Elliott, W. P., R. J. Ross, and D. J. Gaffen, 1995: Water vapor trends over North America. Preprints, *Sixth Symp. on Global Change Studies*, Dallas, TX, Amer. Meteor. Soc., 185–186.
- Giorgi, F., and G. T. Bates, 1989: The climatological skill of a regional model over complex terrain. *Mon. Wea. Rev.*, **117**, 2325–2347.
- , and C. Shields, 1999: Tests of precipitation parameterizations available in latest version of NCAR regional climate model (RegCM) over continental United States. *J. Geophys. Res.*, **104**, 6353–6375.
- , G. T. Bates, and S. Nieman, 1993: The multiyear surface climatology of a regional atmospheric model over the western United States. *J. Climate*, **6**, 75–95.
- , C. S. Brodeur, and G. T. Bates, 1994: Regional climate change scenarios over the United States produced with a nested regional climate model: Spatial and seasonal characteristics. *J. Climate*, **7**, 375–399.
- , J. W. Hurrell, M. R. Marinucci, and M. Beniston, 1997: Elevation dependency of the surface climate signal: A model study. *J. Climate*, **10**, 288–296.
- Goodridge, J. D., 1994: A study of 1000 year storms in California. *Predicting Heavy Rainfall Events in California: A Symposium to Share Weather Pattern Knowledge*, Rocklin, CA, Sierra College, 142 pp.
- Groisman, P. Ya., R. W. Knight, and T. R. Karl, 2001: Heavy precipitation and high stream flow in the contiguous United States: Trends in the twentieth century. *Bull. Amer. Meteor. Soc.*, **82**, 219–246.
- Gutman, G., and A. Ignatov, 1998: Derivation of green vegetation fraction from NOAA/AVHRR for use in numerical weather prediction models. *Int. J. Remote Sens.*, **19**, 1533–1543.
- Harshvardhan, R. Davis, D. A. Randall, and T. Corsetti, 1987: A fast radiation parameterization scheme for atmospheric circulation models. *J. Geophys. Res.*, **92** (D1), 1009–1016.
- Hong, S.-Y., and H.-L. Pan, 1998: Convective trigger function for a mass flux cumulus parameterization scheme. *Mon. Wea. Rev.*, **126**, 2599–2620.
- Houghton, J. T., L. G. Meira Filho, B. A. Callandar, N. Harris, A. Kattenberg, and K. Maskell, Eds., 1996: *Climate Change 1995: The Science of Climate Change*. Cambridge University Press, 572 pp.
- Johns, T. C., R. E. Carnell, J. F. Crossley, J. M. Gregory, J. F. B. Mitchell, C. A. Senior, S. F. B. Tett, and R. A. Wood, 1997: The second Hadley Centre coupled ocean-atmosphere GCM: Model description, spinup and validation. *Climate Dyn.*, **13**, 103–134.
- Kim, J., 1997: Precipitation and snow budget over the southwestern United States during the 1994–1995 winter season in a mesoscale model simulation. *Water Resour. Res.*, **33**, 2831–2839.
- , 2001: A nested modeling study of elevation-dependent climate

- change signals in California induced by increased atmospheric CO₂. *Geophys. Res. Lett.*, **28**, 2951–2954.
- , and M. Ek, 1995: A simulation of the surface energy budget and soil water content over the HAPEX/MOBILHY forest site. *J. Geophys. Res.*, **100** (D10), 20 845–20 854.
- , and S. Soong, 1996: Simulation of a precipitation event in the western United States. *Regional Impacts of Global Climate Change: Assessing Change and Response at the Scales that Matter*, S. J. Ghan et al., Eds., Batelle, 73–84.
- , N. Miller, A. K. Guetter, and K. P. Georgakakos, 1998: River flow response to precipitation and snow budget in California during the 1994/95 winter. *J. Climate*, **11**, 2376–2386.
- , —, J. Farrara, and S. Hong, 2000: A season precipitation and streamflow hindcast and prediction study in the western United States during the 1997/98 winter season using a dynamic downscaling system. *J. Hydrometeorol.*, **1**, 311–329.
- Kyriakidis, P. C., J. Kim, and N. Miller, 2001: Geostatistical mapping of precipitation using atmospheric and terrain characteristics. *J. Appl. Meteorol.*, **40**, 1855–1877.
- Leung, L. R., and S. J. Ghan, 1999a: Pacific Northwest climate sensitivity simulated by a regional climate model driven by a GCM. Part I: Control simulations. *J. Climate*, **12**, 2010–2030.
- , and —, 1999b: Pacific Northwest climate sensitivity simulated by a regional climate model driven by a GCM. Part II: 2×CO₂ simulations. *J. Climate*, **12**, 2031–2053.
- Lorenz, E., 1960: Energy and numerical weather prediction. *Tellus*, **12**, 364–373.
- Mahrt, L., and H.-L. Pan, 1984: A two-layer model of soil hydrology. *Bound.-Layer Meteorol.*, **29**, 1–20.
- Miller, N., and J. Kim, 1996: Numerical prediction of precipitation and river flow over the Russian River watershed during the January 1995 California storms. *Bull. Amer. Meteor. Soc.*, **77**, 101–105.
- Mitchell, J., T. Jones, J. Gregory, and S. Tett, 1995: Climate response to increasing levels of greenhouse gases and sulfate aerosols. *Nature*, **376**, 501–504.
- Pan, H., and L. Mahrt, 1987: Interaction between soil hydrology and boundary layer development. *Bound.-Layer Meteorol.*, **38**, 185–202.
- , and W. Wu, 1995: Implementing a mass flux convection parameterization package for the NCEP medium-range forecast model. NMC Office Note, 40 pp. [Available from NCEP/EMC, 5200 Auth Rd., Camp Springs, MD 20746.]
- Santer, B. D., and Coauthors, 1995: Detection of climate change and attribution of causes. *Climate Change 1995: The Science of Climate Change*, Cambridge University Press, 407–443.
- Soong, S., and J. Kim, 1996: Simulation of a heavy wintertime precipitation event in California. *Climatic Change*, **32**, 55–77.
- Starr, D., and S. Cox, 1985: Cirrus clouds. Part I: A cirrus cloud model. *J. Atmos. Sci.*, **42**, 2663–2681.
- Stephens, G., 1978: Radiation profiles in extended water clouds. II: Parameterization schemes. *J. Atmos. Sci.*, **35**, 2123–2132.
- Takacs, L., 1985: A two-step scheme for the advection equation with minimized dissipation and dispersion errors. *Mon. Wea. Rev.*, **113**, 1050–1065.
- Wilby, R. L., T. M. L. Wigley, D. Conway, P. D. Jones, B. C. Hewiston, J. Main, and D. S. Wilks, 1998: Statistical downscaling of general circulation model output: A comparison of methods. *Water Resour. Res.*, **34**, 2995–3008.